Topology optimization of sound absorbing layer for the mid-frequency vibration of vibro-acoustic systems

Ruxin Gao[a], Yahui Zhang[a*], David Kennedy[b]

[a] *State Key Laboratory of Structural Analysis for Industrial Equipment, Department of Engineering Mechanics, International Center for Computational Mechanics, Dalian University of Technology, Dalian 116023, PR China;*

[b] *School of Engineering, Cardiff University, Cardiff CF24 3AA, Wales, UK*

Corresponding author:

Dr. Y. H. Zhang

State Key Laboratory of Structural Analysis for Industrial Equipment, Department of Engineering Mechanics, Dalian University of Technology, Dalian 116023, PR China

Email: zhangyh@dlut.edu.cn

Tel: +86 411 84706337

Fax: +86 411 84708393

Abstract

Due to the significant difference of dynamic properties between the fluid medium and the structure, when a vibro-acoustic system is subjected to a higher frequency excitation, it may typically exhibit mid-frequency behavior which involves different wavelength deformations and is very sensitive to the uncertainties of the system. This paper deals with optimized distribution of a sound absorbing layer for the mid-frequency vibration of vibro-acoustic systems by using hybrid boundary element analysis and statistical energy analysis. Based on the SIMP approach an artificial sound absorbing material model is suggested and the relative densities of the sound absorbing material are taken as design variables. The sound pressure level at a specified point in the acoustic cavity is to be minimized by distributing a given amount of sound absorbing material. An efficient direct differentiation scheme for the response sensitivity analysis is proposed. Then the optimization problem is solved by using the method of moving asymptotes. A numerical example illustrates the validity and effectiveness of the present optimization model. Impact of the excitation frequency on optimized topology is also discussed.

Keywords: Mid-frequency; Vibro-acoustic system; Sound absorbing layer; Boundary element; Statistical energy analysis; Dynamic topology optimization

1 Introduction

Vibro-acoustic systems are widely used in vehicles such as automobiles, trains, ships and rocket launchers. These vehicles may be subjected to complex environmental excitations during their operation, resulting in strong structural vibration and harmful high noise levels. Early studies on vibration and noise control (see e.g. Christensen et al. 1998a, b) mainly alter the shape and size of system components to control the generation of noise at the sound source. With the development of topology optimization techniques (Sigmund 2001; Bendsøe and Sigmund 2003), more and more researchers began to study the noise control problem of vibro-acoustic systems by using topology optimization techniques. Yoon et al. (2007) dealt with the problem of topology optimization of vibro-acoustic systems using a mixed finite element (FE) formulation (Zienkiewicz and Taylor 2000; Bathe 2008), in which the acoustic cavity is enclosed by a finite boundary. Kook et al. (2012) proposed a design method for acoustical topology optimization considering human hearing characteristics. Shu et al. (2014) studied the topology optimization of vibro-acoustic systems for minimizing sound pressure by using the level set method. To date, the studies on topology optimization of vibro-acoustic systems have been mainly focused on the optimized distribution of structural materials, while the topology optimization of damping or sound absorbing layers has been rarely involved.

However, the design of a large vehicle should not only consider vibration and noise reduction, but also meet other design requirements including stiffness, strength, stability,

1   aerodynamics and hydrodynamics. Therefore, design methods for vibration and noise

2   reduction by finding the optimized layout of structural material have some limitations. At

3   present, a commonly used method is to place damping material on the surface of a

4   structure and sound absorbing material on the sound propagation path to reduce the

5   acoustic radiation and the reflection or transmission of sound waves, respectively.

6   However, a large area of damping or sound absorbing material will cause a sharp increase

7   in system weight, which will not only affect the system performance but also increase the

8   manufacturing cost. In view of the above situation, topology optimization techniques are

9   used to obtain the optimized layout of damping or sound absorbing layers in a vibro-

10   acoustic system. Dühring et al. (2008) studied the optimized placement of damping panels

11   on walls of acoustic cavities by using the solid isotropic material with penalization (SIMP)

12   method (Sigmund 2001; Bendsøe and Sigmund 2003). The sound level can be

13   significantly reduced by optimizing the distribution of the sound absorbing and reflecting

14   material. Akl et al. (2009) developed a mathematical model to simulate fluid-structure

15   interactions based on FE method. A good agreement was obtained between the results

16   obtained from the mathematical model and those from the experiment. Zhang and Kang

17   (2013) presented a topology optimization model to obtain the optimized layout of a

18   damping layer for minimizing the acoustic radiation of damped thin-walled structures. In

19   their paper, the dynamic coupling between the acoustic medium and the structure is

20   neglected. Then considering the velocity response of the structure which is calculated by

1   FE method as an acoustic excitation, the sound pressure at a reference point is obtained

2   by using the boundary element (BE) method (Ciskowski and Brebbia 1991; Wu 2000).

3   They also proposed a sensitivity analysis scheme using the adjoint variable method. Zhao

4   et al. (2017) studied the optimized design of sound absorbing material distribution within

5   sound barrier structures based on the BE method and the optimality criteria method. A

6   smoothed Heaviside-like function was developed to help the SIMP method to obtain a

7   clear 0-1 distribution. The optimized distribution of the sound absorbing material is

8   strongly frequency dependent according to the results obtained by authors, and the

9   optimization in a frequency band was suggested. Du and Olhoff (2007, 2010) studied the

10   topology optimization problem of vibrating bi-material elastic structures placed in an

11   acoustic medium for minimizing the acoustic radiation and gave a corresponding

12   sensitivity analysis scheme. Their papers assumed that the vibration frequency of a

13   structure has a sufficiently high value, so that the radiation impedance at the structure

14   boundary is approximately equal to the characteristic impedance of the acoustic medium

15   (Lax and Feshbach 1947; Herrin et al. 2003). Thus the sound pressure in the acoustic field

16   can be easily obtained by using a high frequency boundary integral equation. Considering

17   that resonance and wave-propagation problems are known to be highly sensitive towards

18   parameter variations and the conventional robust topology optimization methods for

19   structural problems are not suitable for the acoustic problem, Christiansen et al. (2015)

20   suggested a new double filter approach and obtained highly robust designs for acoustic

1   problem. Christiansen and Sigmund (2015) provide the experimental validation of an

2   acoustic cavity designed using topology optimization with the goal of minimizing the

3   sound pressure locally for monochromatic excitation.

4   Based on deterministic methods, such as the FE method, several of the papers

5   mentioned above studied the topology optimization of vibro-acoustic systems. As the

6   frequency increases, the deformation wavelength of the system components will decrease

7   significantly. A fine mesh is required to capture the detailed deformation, typically six to

8   eight elements per wavelength (Simmons 1991; Steel and Craik 1994), which leads to a

9   large number of degrees of freedom (DOF). The computational cost of element-based

10   techniques typically increases due to decreasing wavelengths and multiple reanalyses in

11   the optimization process (Cotoni et al. 2007). Moreover, as the frequency increases, the

12   response of a system will be more and more sensitive to the uncertainties which are

13   inevitably generated during the manufacturing process. Systems with the same nominal

14   geometric and material parameters may produce different responses. At this point, it

15   makes no sense to analyze only one system, and an estimate of average behavior of an

16   ensemble of similar systems with the same nominal properties might be preferred

17   (Ladeveze et al. 2012). As a common statistical method, statistical energy analysis (SEA)

18   (Lyon and DeJong 1995), can give an average prediction for the statistical behavior of

19   systems with little computational cost. However, the assumptions introduced in SEA can

20   only be satisfied when the system is subjected to sufficiently high frequencies (Lyon and

1　DeJong 1995; Langley 1989a). In addition, based on SEA the properties of a system may

2　be highly generalized as some parameters are independent of the material topology layout,

3　which makes topology optimization impossible.

4　　Due to the significant difference of dynamic properties between the fluid medium

5　and the structure, when a vibro-acoustic system is subjected to a higher frequency

6　excitation, it may typically exhibit mid-frequency behavior in which some subsystems

7　are large compared with a wavelength, while others are small compared with a

8　wavelength (Shorter and Langley 2005b). At present, neither the FE method nor SEA can

9　describe the motion of vibro-acoustic systems well. To address this situation, three types

10　of improved methods have been proposed for the mid-frequency vibration of complex

11　systems. The first type aims to extend the effective frequency range of traditional

12　deterministic methods to the mid-frequency domain (see e.g. Langley 1989b; Van

13　Vinckenroy and De Wilde 1995; Harari and Avraham 1997; Pluymers et al. 2007; Hinke

14　et al. 2009; Ma et al. 2015b). The second type aims to relax the assumptions in SEA to

15　extend its application to the mid-frequency domain (see e.g. Keane and Price 1987;

16　Langley 1992; Maxit and Guyader 2003; Mace 2005). The third type combines the

17　deterministic and statistical methods to develop a hybrid model for the mid-frequency

18　vibration of complex systems (see e.g. Zhao and Vlahopoulos 2000; Shorter and Langley

19　2005a, b; Ji et al. 2006; Vergote et al. 2011; Zhu et al. 2014; Ma et al. 2015a; Gao et al.

20　2018). As the most popular hybrid approach, the hybrid FE-SEA method proposed by

1   Shorter and Langley (2005b) divides a complex system into a number of deterministic

2   and statistical subsystems according to the deformation wavelength. The so-called

3   deterministic subsystem which is subjected to long wavelength deformation can be

4   modeled by using the FE method, while the so-called statistical subsystem which is

5   subjected to short wavelength deformation can be modeled by using SEA. The dynamic

6   coupling between the two types of subsystems is described as the reflection and

7   transmission of the vibration wave. Based on the diffuse field reciprocity principle

8   (Shorter and Langley 2005a), a non-iterative relationship between the deterministic and

9   statistical subsystems can be established. Due to the combination of the FE method and

10   SEA, the hybrid FE-SEA method can give an average prediction for the mid-frequency

11   vibration and deal with actual engineering systems. Considering the BE method to

12   describe the motion of an acoustic cavity, Gao et al. (2018) proposed the hybrid BE-SEA

13   method for the mid-frequency vibration of vibro-acoustic systems. Due to the nature of

14   the BE method, the hybrid BE-SEA method not only satisfies the Sommerfeld radiation

15   condition at infinity for exterior acoustic problem, but is also more efficient in the

16   modeling stage. Since hybrid approaches are more appropriate than the traditional method

17   for the mid-frequency of complex systems, Muthalif and Langley(2012) studied the active

18   control of mid-frequency vibration by using the hybrid FE-SEA method as an analysis

19   tool. The optimized skyhook damping value and its location were calculated by using the

20   MATLAB GADS toolbox with combined pattern search and genetic algorithms. By using

the hybrid FE-wave based (WB) method, Goo et al. (2017) proposed an efficient topology

optimization method for bounded acoustic problems. Their method employs the FE

method and WB method to respectively model the design and non-design domains to

increase computational efficiency and can thus be applied to higher frequency

applications that conventional method takes considerable computation time to manage.

The present work studies optimized distribution of a sound absorbing layer for the

mid-frequency vibration of vibro-acoustic systems by using the hybrid BE-SEA method.

In the topology optimization model, an artificial sound absorbing material model is

established by employing the SIMP approach. The design objective is the sound pressure

level at a specified point in the acoustic cavity, and the design variables are the relative

densities of the sound absorbing material. The corresponding sensitivity analysis scheme

is derived by direct differentiation. The basic principles of the hybrid BE-SEA method

are outlined in Section 2. The topology optimization problem formulation and the

corresponding sensitivity analysis scheme are developed in Section 3. In Section 4, a

numerical example is presented to illustrate the efficiency of the hybrid BE-SEA method

and the validity of the proposed topology optimization model. The impact of the

excitation frequency on optimized topology is also discussed. Finally, conclusions are

given in Section 5.

2 Basic principles of hybrid BE-SEA method

The hybrid BE-SEA method was proposed by Gao et al. (2018) for the mid-frequency vibration of vibro-acoustic systems based on the concept of the hybrid FE-SEA method. Due to the use of the BE method, the hybrid BE-SEA method provided an appropriate model with modeling advantages when the deterministic part of the model is a relatively large acoustic domain.

Without loss of generality, this section demonstrates the basic principles of the hybrid BE-SEA method. In a vibro-acoustic system, the fluid is confined in a bounded acoustic domain Ω, as shown in Fig. 1, of which the boundary surface Γ_a contains a velocity surface Γ_v, an impedance (sound absorbing) surface Γ_Z and an elastic thin-walled structural surface Γ_s. The velocity and impedance boundary conditions are expressed by a generalized equation which can be written as (Wu 2000)

$$\mathbf{v}_n = \mathbf{C}_\beta \mathbf{C}_\gamma - \mathbf{C}_\beta \mathbf{C}_\alpha \mathbf{p} \tag{1}$$

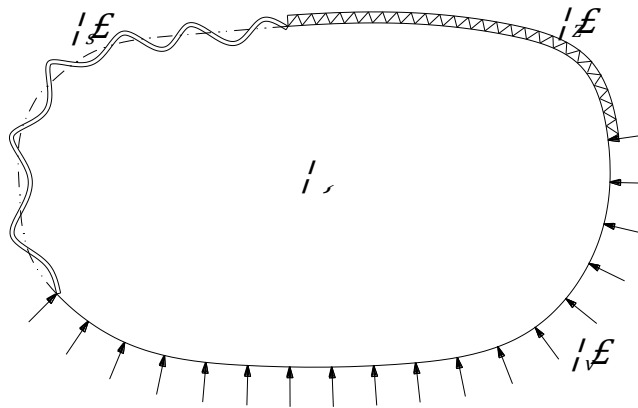Fig. 1 Coupled vibro-acoustic system. Ω, acoustic domain; Γ_v, velocity boundary surface; Γ_Z, impedance boundary surface; Γ_s, elastic thin-structural surface.

1   where the vectors $\mathbf{p}$ and $\mathbf{v}_n$ respectively represent the sound pressures and normal

2   velocities at nodal points on the boundary of the acoustic cavity. $\mathbf{C}_\alpha$ and $\mathbf{C}_\beta$ are

3   constraint coefficient diagonal matrices corresponding to sound pressure and normal

4   velocity, respectively. $\mathbf{C}_\gamma$ is a constraint coefficient vector. The hybrid BE-SEA method

5   (Gao et al. 2018) may be employed for the mid-frequency vibration of the system. The

6   acoustic cavity modeled by the BE method is treated as the deterministic subsystem, while

7   the thin-walled structure modeled by SEA is treated as the statistical subsystem.

8   According to the hybrid BE-SEA method, the response of the statistical thin-walled

9   structure is viewed as the superposition of the direct and reverberant fields (see Shorter

10   and Langley 2005a). Considering the velocity and impedance boundary conditions and

11   the coupling interaction between the acoustic cavity and the direct field of the thin-walled

12   structure, the governing equation of the system can be written as (Gao et al. 2018)

13

$$\begin{bmatrix} \widetilde{\mathbf{H}} & -\mathrm{i}\omega\mathbf{G}\mathbf{T} \\ -\mathbf{A} & \mathbf{D}_{\mathrm{dir}} \end{bmatrix} \begin{Bmatrix} \mathbf{p} \\ \mathbf{u} \end{Bmatrix} = \begin{Bmatrix} \mathbf{G}\bar{\mathbf{v}}_n \\ \mathbf{0} \end{Bmatrix} + \begin{Bmatrix} \mathbf{0} \\ \mathbf{f}_{\mathrm{rev}}^{\mathrm{s}} \end{Bmatrix} \tag{2}$$

14

15   where $\bar{\mathbf{v}}_n = \mathbf{C}_\beta\mathbf{C}_\gamma$, $\widetilde{\mathbf{H}} = \mathbf{H} + \mathbf{G}\mathbf{C}_\beta\mathbf{C}_\alpha$, $\mathbf{H}$ and $\mathbf{G}$ are the influence matrices of sound

16   pressure and normal velocity, respectively. $\mathbf{D}_{\mathrm{dir}}$ and $\mathbf{u}$ are the dynamic stiffness matrix

17   and displacement vector of the direct field of the thin-walled structure, respectively. $\mathbf{f}_{\mathrm{rev}}^{\mathrm{s}}$

18   is the vector of the blocked reverberant forces. $\mathbf{A}$ is a coupling coefficient matrix which

19   converts the sound pressure vector of the acoustic cavity into the nodal force vector of

20   the direct field of the thin-walled structure. $\mathbf{T}$ is the transformation matrix resulting from

11

1   the non-conforming grids appearing at the fluid-structure coupling face, ω is the angular

2   frequency, and $i = \sqrt{-1}$. For the sake of simplicity, Equation (2) will be written as

3

$$\mathbf{D}_{\text{tot}}\mathbf{q} = \mathbf{f}_{\text{ext}} + \mathbf{f}_{\text{rev}} \tag{3}$$

4

5   where $\mathbf{D}_{\text{tot}} = \begin{bmatrix} \widetilde{\mathbf{H}} & -i\omega\mathbf{GT} \\ -\mathbf{A} & \mathbf{D}_{\text{dir}} \end{bmatrix}$ and $\mathbf{q} = \begin{Bmatrix} \mathbf{p} \\ \mathbf{u} \end{Bmatrix}$ respectively represent the total dynamic

6   stiffness matrix and the vector of all deterministic DOF. $\mathbf{f}_{\text{ext}} = \begin{Bmatrix} \mathbf{G}\bar{\mathbf{v}}_n \\ \mathbf{0} \end{Bmatrix}$ and $\mathbf{f}_{\text{rev}} = \begin{Bmatrix} \mathbf{0} \\ \mathbf{f}_{\text{rev}}^s \end{Bmatrix}$

7   respectively represent the vectors of all external and blocked reverberant forces.

8   If there is sufficient uncertainty in the statistical subsystem, the statistics of the

9   blocked reverberant force tend to zero (see Shorter and Langley 2005a). Rewriting

10   equation (3) in cross-spectral form and averaging over an ensemble of statistical thin-

11   walled structures gives

12

$$\mathbf{S}_{qq} = \langle \mathbf{q}\mathbf{q}^{\text{H}} \rangle = \begin{bmatrix} \mathbf{S}_{pp} & \mathbf{S}_{pu} \\ \mathbf{S}_{up} & \mathbf{S}_{uu} \end{bmatrix} = \mathbf{S}_{qq}^{\text{ext}} + \mathbf{S}_{qq}^{\text{rev}} \tag{4}$$

13

14   where $\mathbf{S}_{qq}$ represents the cross-spectrum matrix of the deterministic DOF. $\#^{\text{H}}$ is the

15   Hermitian transpose of $\#$, and $\langle \# \rangle$ is the ensemble average of $\#$. The subscripts p and

16   u stand for the DOF of the acoustic cavity and the direct field of the thin-walled structure.

17   Also

18

$$\mathbf{S}_{qq}^{\text{ext}} = \mathbf{D}_{\text{tot}}^{-1}\mathbf{S}_{ff}^{\text{ext}}\mathbf{D}_{\text{tot}}^{-\text{H}} = \begin{bmatrix} \mathbf{S}_{pp}^{\text{ext}} & \mathbf{S}_{pu}^{\text{ext}} \\ \mathbf{S}_{up}^{\text{ext}} & \mathbf{S}_{uu}^{\text{ext}} \end{bmatrix} \tag{5}$$

19

$$\mathbf{S}_{qq}^{\text{rev}} = \mathbf{D}_{\text{tot}}^{-1}\mathbf{S}_{ff}^{\text{rev}}\mathbf{D}_{\text{tot}}^{-\text{H}} = \begin{bmatrix} \mathbf{S}_{pp}^{\text{rev}} & \mathbf{S}_{pu}^{\text{rev}} \\ \mathbf{S}_{up}^{\text{rev}} & \mathbf{S}_{uu}^{\text{rev}} \end{bmatrix} \tag{6}$$

1 where $\mathbf{S}_{ff}^{\text{ext}} = \langle \mathbf{f}_{\text{ext}} \mathbf{f}_{\text{ext}}{}^{\text{H}} \rangle$ and $\mathbf{S}_{ff}^{\text{rev}} = \langle \mathbf{f}_{\text{rev}} \mathbf{f}_{\text{rev}}{}^{\text{H}} \rangle$ respectively represent the cross-

2 spectrum matrices of the total external and blocked reverberant forces. $\#^{-\text{H}}$ represents

3 the Hermitian transpose of the inverse matrix. Considering the diffuse field reciprocity

4 principle (see Shorter and Langley 2005a), equation (6) can be rewritten in terms of the

5 reverberant field energy E and the modal density n_{m} of the thin-walled structure as

6

$$\mathbf{S}_{qq}^{\text{rev}} = \frac{E}{n_{\text{m}}} \frac{4}{\pi\omega} \mathbf{\Upsilon} \tag{7}$$

7

8 where

9

$$\mathbf{\Upsilon} = \mathbf{D}_{\text{tot}}^{-1} \text{Im}\{\widetilde{\mathbf{D}}_{\text{dir}}\} \mathbf{D}_{\text{tot}}^{-\text{H}} = \begin{bmatrix} \mathbf{\Upsilon}_{pp} & \mathbf{\Upsilon}_{pu} \\ \mathbf{\Upsilon}_{up} & \mathbf{\Upsilon}_{uu} \end{bmatrix} \tag{8}$$

10

11 with

12

$$\widetilde{\mathbf{D}}_{\text{dir}} = \begin{bmatrix} \mathbf{0} & \mathbf{0} \\ \mathbf{0} & \mathbf{D}_{\text{dir}} \end{bmatrix} \tag{9}$$

13

14   The cross-spectrum matrix of the deterministic DOF $\mathbf{S}_{qq}$ can be obtained by using

15 equations (4)-(9). The only unknown quantity E, at this time, can be calculated by

16 employing the power balance equation of the reverberant field of the thin-walled structure,

17 which is given by (see Gao et al. 2018)

18

$$(h_{\text{out}}^{\text{rev}} + h_{\text{diss}}) \frac{E}{n_{\text{m}}} = P_{\text{in}} \tag{10}$$

19

20 Here, $h_{\text{out}}^{\text{rev}}$ and h_{diss} respectively represent the total energy leaving the reverberant

1 field of the thin-walled structure into the acoustic cavity and the total energy dissipating

2 by the damping of the thin-walled structure per unit modal energy density in the

3 reverberant field of the thin-walled structure. $P_{\text{in}} = P_{\text{in}}^{\text{dir}} + P_{\text{in}}^{\text{ext}}$ is the total power input

4 to the statistical thin-walled structure, where $P_{\text{in}}^{\text{dir}}$ is the power arising from the force

5 applied to the acoustic cavity and $P_{\text{in}}^{\text{ext}}$ is the power caused by other sources applied

6 directly to the statistical thin-walled structure. The above parameters can be expressed as

7

$$P_{\text{in}}^{\text{dir}} = \frac{\omega}{2} \sum_{ij} \text{Im}\{\mathbf{D}_{\text{dir},ij}\}(\mathbf{S}_{uu}^{\text{ext}})_{ij} \tag{11}$$

8

$$h_{\text{diss}} = \omega n_{\text{m}} \eta \tag{12}$$

9

$$h_{\text{out}}^{\text{rev}} = \frac{2}{\pi} \text{Re}\left\{ -i \sum_{ij} \mathbf{C}_{\text{sa},ij}(\mathbf{\Upsilon}_{up})_{ij}^* \right\} \tag{13}$$

10

11 where η is the damping loss factor of the thin-walled structure, $\mathbf{C}_{\text{sa}}$ is a coupling

12 coefficient matrix which connects the shape functions of the grids of the acoustic cavity

13 and the direct field of the thin-walled structure (see Gao et al. 2018). $\#^*$ stands for the

14 complex conjugate of $\#$.

15   By substituting equations (11)-(13) into equation (10), the ensemble average energy

16 of the reverberant field can be obtained. The energy of the direct field of the thin-walled

17 structure can be neglected (see Shorter and Langley 2005b). Hence, by using equations

18 (4)-(9), $\mathbf{S}_{qq}$ can be calculated. Selecting some points inside the acoustic cavity and

calculating the corresponding coefficient matrices $\mathbf{g}$ of sound pressure and $\mathbf{h}$ of normal velocity, the cross-spectrum matrix of sound pressure at these points can be expressed as (see Gao et al. 2018)

$$\mathbf{S}_{pp}^{\text{in}} = \omega^2(\mathbf{g}\mathbf{T}\mathbf{S}_{uu}\mathbf{T}^{\text{H}}\mathbf{g}^{\text{H}}) + \mathrm{i}\omega(\mathbf{\Delta} - \mathbf{\Delta}^{\text{H}}) + \mathbf{\Xi} - \mathbf{\Pi} - \mathbf{\Pi}^{\text{H}} \tag{14}$$

where

$$\mathbf{\Delta} = \mathbf{g}\mathbf{Q}\mathbf{g}^{\text{H}} + \tilde{\mathbf{h}}\mathbf{S}_{pu}\mathbf{T}^{\text{H}}\mathbf{g}^{\text{H}} \tag{15}$$

$$\mathbf{\Xi} = \mathbf{g}\mathbf{S}_{\bar{v}_{\mathrm{n}}\bar{v}_{\mathrm{n}}}\mathbf{g}^{\text{H}} + \tilde{\mathbf{h}}\mathbf{S}_{pp}\tilde{\mathbf{h}}^{\text{H}} \tag{16}$$

$$\mathbf{\Pi} = \mathbf{g}\mathbf{S}_{\bar{v}_{\mathrm{n}}p}\tilde{\mathbf{h}}^{\text{H}} \tag{17}$$

with

$$\mathbf{S}_{\bar{v}_{\mathrm{n}}\bar{v}_{\mathrm{n}}} = \langle \bar{\mathbf{v}}_{\mathrm{n}}\bar{\mathbf{v}}_{\mathrm{n}}^{\text{H}} \rangle \tag{18}$$

$$\tilde{\mathbf{h}} = \mathbf{h} + \mathbf{g}\mathbf{C}_{\beta}\mathbf{C}_{\alpha} \tag{19}$$

$$\mathbf{S}_{\bar{v}_{\mathrm{n}}p} = \mathbf{G}^{-1}\tilde{\mathbf{H}}\mathbf{S}_{pp} - \mathrm{i}\omega\mathbf{T}\mathbf{S}_{up} \tag{20}$$

$$\mathbf{Q} = \mathbf{T}\mathbf{S}_{u\bar{v}_{\mathrm{n}}} = \left(\mathbf{G}^{-1}\tilde{\mathbf{H}}\mathbf{S}_{\bar{v}_{\mathrm{n}}p}^{\text{H}} - \mathbf{S}_{\bar{v}_{\mathrm{n}}\bar{v}_{\mathrm{n}}}\right)/\mathrm{i}\omega \tag{21}$$

Now inserting equations (15)-(21) into equation (14), $\mathbf{S}_{pp}^{\text{in}}$ can be obtained, and then the sound pressure level at the points inside the acoustic cavity can be calculated.
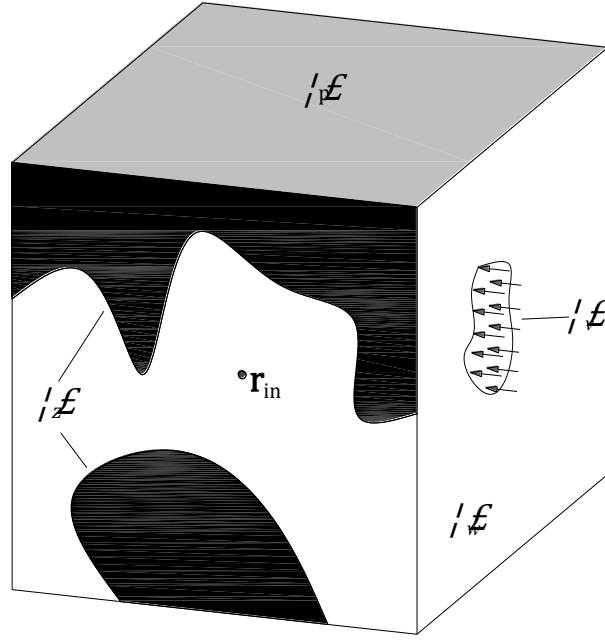
1

2　　Fig. 2　A vibro-acoustic system with surface sound absorbing layer. Γ_p, a thin plate;

3　　Γ_z, the layer of sound absorbing material; Γ_v, the domain subjected to external

4　　excitation; Γ_w, the acoustically rigid walls; $\mathbf{r}_{in}$, a reference point inside the acoustic

5　　cavity.

6　3 Topology optimization problem formulation

7　3.1 Topology optimization model

8　　　　Considering a vibro-acoustic system consisting of a deterministic acoustic cavity

9　　and a statistical thin plate as shown in Fig. 2, the acoustic cavity is a cuboid domain

10　　coupled with a thin plate on the upper surface. A layer of sound absorbing material is

11　　attached to the front surface of the acoustic cavity domain, and a velocity excitation is

12　　applied over a region on its right surface. The other regions of the boundary of the acoustic

13　　cavity domain are assumed to be acoustically rigid walls. By employing the hybrid BE-

14　　SEA method for the mid-frequency vibration of the vibro-acoustic system, this section

1   deals with the optimized layout of a given amount of sound absorbing material within a

2   prescribed design domain for minimizing the sound pressure level at a specified point

3   inside the cavity. The topology problem can be thus formulated as

4

$$
\left.
\begin{array}{ll}
\text{find} & \boldsymbol{\rho} = \{\rho_1 \quad \rho_2 \quad \cdots \quad \rho_{m_Z}\}^{\mathrm{T}} \\
\text{min} & \tilde{S}_{pp}^{\mathrm{in}}(\mathbf{r}_{\mathrm{in}}) = \langle p^* p \rangle \\
\text{s.t.} & \displaystyle\sum_{k=1}^{m_Z} \rho_k V_k^0 - f_V \sum_{k=1}^{m_Z} V_k^0 \leq 0 \\
& 0 < \rho_{\mathrm{min}} \leq \rho_k \leq 1 \ (k = 1, \dots, m_Z)
\end{array}
\right\}
\tag{22}
$$

5

6   where $\boldsymbol{\rho}$ is the vector of the relative density design variables describing layout of the

7   sound absorbing material. m_Z represents the total number of boundary elements in the

8   design domain, and each element has one design variable. $\tilde{S}_{pp}^{\mathrm{in}}(\mathbf{r}_{\mathrm{in}})$ represents the

9   objective function and is a diagonal element of $\mathbf{S}_{pp}^{\mathrm{in}}$ representing the power spectral

10   density of sound pressure (PSDSP) at a specified point $\mathbf{r}_{\mathrm{in}}$ inside the acoustic cavity. It

11   is important to point out that the objective function can also be written as the sum of the

12   PSDSPs at more points (i.e. $f = \sum \langle p_i^* p_i \rangle, i = 1,2 \dots n$) to obtain an overall sound

13   pressure reduction in the acoustic cavity (Du and Olhoff 2010). f_V represents the volume

14   fraction and V_k^0 is the volume of sound absorbing material in the kth boundary element

15   when $\rho_k = 1$. ρ_{min} is the lower bound of the relative density variables, which is set to

16   be 10^-6 to avoid possible numerical singularity.

17   Based on the framework of the SIMP approach, $\mathbf{C}_\alpha$, $\mathbf{C}_\beta$ and $\mathbf{C}_\gamma$ can be

18   respectively written as

1

$$\mathbf{C}_\alpha = \sum_{k=1}^{m_Z} (\rho_k)^N \mathbf{R}_{\alpha,Z}^{(k)} \tag{23}$$

2

$$\mathbf{C}_\beta = \mathrm{diag}\{\mathbf{E}_v - \mathbf{E}_Z\} \tag{24}$$

3

$$\mathbf{C}_\gamma = \sum_{k=1}^{m_v} \mathbf{v}_0^{(k)} \tag{25}$$

4

5   where $\mathbf{R}_{\alpha,Z}^{(k)}$ is the admittance matrix of the kth element of the sound absorbing layer.

6   The penalty factor $N > 1$ is set to be $N = 3$ in this study. $\mathbf{E}_v$ and $\mathbf{E}_Z$ are location vectors

7   corresponding to velocity and impedance boundary conditions, respectively. $\mathbf{v}_0^{(k)}$ is the

8   velocity vector of the kth element of the velocity surface, and m_v represents the total

9   number of boundary elements on the velocity surface. From equations (24)-(25), it is clear

10   that $\mathbf{C}_\beta$ and $\mathbf{C}_\gamma$ remain unchanged during the topology optimization process.

11   **3.2 Sensitivity analysis**

12   For solving the optimization model of equation (22) with a gradient-based

13   mathematical programming algorithm, it is necessary to perform sensitivity analysis of

14   the objective and constraint functions with respect to the design variables. The sensitivity

15   equation for the PSDSP is derived by direct differentiation, as follows.

16   Differentiating the objective function in equation (22) with respect to the kth design

17   variable gives $\frac{\partial \tilde{S}_{pp}^{\mathrm{in}}}{\partial \rho_k}$, a diagonal element of $\frac{\partial \mathbf{S}_{pp}^{\mathrm{in}}}{\partial \rho_k}$ which can be expressed as

18

$$\frac{\partial \mathbf{S}_{pp}^{\text{in}}}{\partial \rho_k} = \omega^2 \left(\mathbf{g} \mathbf{T} \frac{\partial \mathbf{S}_{uu}}{\partial \rho_k} \mathbf{T}^{\text{H}} \mathbf{g}^{\text{H}} \right) + \text{i}\omega \left[\frac{\partial \boldsymbol{\Delta}}{\partial \rho_k} - \left(\frac{\partial \boldsymbol{\Delta}}{\partial \rho_k} \right)^{\text{H}} \right] + \frac{\partial \boldsymbol{\Xi}}{\partial \rho_k} - \frac{\partial \boldsymbol{\Pi}}{\partial \rho_k} - \left(\frac{\partial \boldsymbol{\Pi}}{\partial \rho_k} \right)^{\text{H}} \quad (26)$$

By using equations (15)-(21), $\frac{\partial \boldsymbol{\Delta}}{\partial \rho_k}$, $\frac{\partial \boldsymbol{\Xi}}{\partial \rho_k}$ and $\frac{\partial \boldsymbol{\Pi}}{\partial \rho_k}$ in equation (26) can be, respectively,

written as

$$\frac{\partial \boldsymbol{\Delta}}{\partial \rho_k} = \mathbf{g} \frac{\partial \mathbf{Q}}{\partial \rho_k} \mathbf{g}^{\text{H}} + \frac{\partial \tilde{\mathbf{h}}}{\partial \rho_k} \mathbf{S}_{pu} \mathbf{T}^{\text{H}} \mathbf{g}^{\text{H}} + \tilde{\mathbf{h}} \frac{\partial \mathbf{S}_{pu}}{\partial \rho_k} \mathbf{T}^{\text{H}} \mathbf{g}^{\text{H}} \quad (27)$$

$$\frac{\partial \boldsymbol{\Xi}}{\partial \rho_k} = \frac{\partial \tilde{\mathbf{h}}}{\partial \rho_k} \mathbf{S}_{pp} \tilde{\mathbf{h}}^{\text{H}} + \tilde{\mathbf{h}} \frac{\partial \mathbf{S}_{pp}}{\partial \rho_k} \tilde{\mathbf{h}}^{\text{H}} + \tilde{\mathbf{h}} \mathbf{S}_{pp} \left(\frac{\partial \tilde{\mathbf{h}}}{\partial \rho_k} \right)^{\text{H}} \quad (28)$$

$$\frac{\partial \boldsymbol{\Pi}}{\partial \rho_k} = \mathbf{g} \frac{\partial \mathbf{S}_{\bar{v}_{\text{n}}p}}{\partial \rho_k} \tilde{\mathbf{h}}^{\text{H}} + \mathbf{g} \mathbf{S}_{\bar{v}_{\text{n}}p} \left(\frac{\partial \tilde{\mathbf{h}}}{\partial \rho_k} \right)^{\text{H}} \quad (29)$$

where

$$\frac{\partial \tilde{\mathbf{h}}}{\partial \rho_k} = \mathbf{g} \mathbf{C}_\beta \frac{\partial \mathbf{C}_\alpha}{\partial \rho_k} \quad (30)$$

$$\frac{\partial \mathbf{S}_{\bar{v}_{\text{n}}p}}{\partial \rho_k} = \mathbf{G}^{-1} \frac{\partial \widetilde{\mathbf{H}}}{\partial \rho_k} \mathbf{S}_{pp} + \mathbf{G}^{-1} \widetilde{\mathbf{H}} \frac{\partial \mathbf{S}_{pp}}{\partial \rho_k} - \text{i}\omega \mathbf{T} \frac{\partial \mathbf{S}_{up}}{\partial \rho_k} \quad (31)$$

$$\frac{\partial \mathbf{Q}}{\partial \rho_k} = \mathbf{T} \frac{\partial \mathbf{S}_{u\bar{v}_{\text{n}}}}{\partial \rho_k} = \left(\mathbf{G}^{-1} \frac{\partial \widetilde{\mathbf{H}}}{\partial \rho_k} \mathbf{S}_{\bar{v}_{\text{n}}p}^{\text{H}} + \mathbf{G}^{-1} \widetilde{\mathbf{H}} \frac{\partial \mathbf{S}_{\bar{v}_{\text{n}}p}^{\text{H}}}{\partial \rho_k} \right) / \text{i}\omega \quad (32)$$

with

$$\frac{\partial \widetilde{\mathbf{H}}}{\partial \rho_k} = \mathbf{G} \mathbf{C}_\beta \frac{\partial \mathbf{C}_\alpha}{\partial \rho_k} \quad (33)$$

Substituting equation (27)-(33) into equation (26), it can be seen that $\frac{\partial \mathbf{S}_{pp}^{\text{in}}}{\partial \rho_k}$ is

1 determined by $\frac{\partial \mathbf{C}_\alpha}{\partial \rho_k}$ and $\frac{\partial \mathbf{S}_{qq}}{\partial \rho_k}$. Differentiating equation (23) with respect to the kth design

2 variable, $\frac{\partial \mathbf{C}_\alpha}{\partial \rho_k}$ can be written as

3

$$\frac{\partial \mathbf{C}_\alpha}{\partial \rho_k} = \sum_{k=1}^{m} N(\rho_k)^{(N-1)} \mathbf{R}_{\alpha,Z}^{(k)} \tag{34}$$

4

5 According to equation (4), $\frac{\partial \mathbf{S}_{qq}}{\partial \rho_k}$ can be written as

6

$$\frac{\partial \mathbf{S}_{qq}}{\partial \rho_k} = \frac{\partial \mathbf{S}_{qq}^{\text{ext}}}{\partial \rho_k} + \frac{\partial \mathbf{S}_{qq}^{\text{rev}}}{\partial \rho_k} \tag{35}$$

7

8 where $\frac{\partial \mathbf{S}_{qq}^{\text{ext}}}{\partial \rho_k}$ and $\frac{\partial \mathbf{S}_{qq}^{\text{rev}}}{\partial \rho_k}$ can be, respectively, obtained by differentiating equations (5) and

9 (7) with respect to the kth design variable and written as

10

$$\frac{\partial \mathbf{S}_{qq}^{\text{ext}}}{\partial \rho_k} = \boldsymbol{\chi}^{(k)} \mathbf{S}_{qq}^{\text{ext}} + \left(\boldsymbol{\chi}^{(k)} \mathbf{S}_{qq}^{\text{ext}} \right)^{\text{H}} \tag{36}$$

11

$$\frac{\partial \mathbf{S}_{qq}^{\text{rev}}}{\partial \rho_k} = \frac{4}{\pi \omega n_{\text{m}}} \left(E \frac{\partial \mathbf{Y}}{\partial \rho_k} + \frac{\partial E}{\partial \rho_k} \mathbf{Y} \right) \tag{37}$$

12

13 with

14

$$\boldsymbol{\chi}^{(k)} = -\mathbf{D}_{\text{tot}}^{-1} \frac{\partial \mathbf{D}_{\text{tot}}}{\partial \rho_k} \tag{38}$$

15

$$\frac{\partial \mathbf{Y}}{\partial \rho_k} = \boldsymbol{\chi}^{(k)} \mathbf{Y} + \left(\boldsymbol{\chi}^{(k)} \mathbf{Y} \right)^{\text{H}} \tag{39}$$

16

17   Derivatives of the thin plate energy and the total dynamic stiffness matrix with

18 respect to the kth design variable respectively appear in equations (37) and (38). By using

19 equations (2), (3) and (33), $\frac{\partial \mathbf{D}_{\text{tot}}}{\partial \rho_k}$ can be expressed as

1

$$\frac{\partial \mathbf{D}_{\text{tot}}}{\partial \rho_k} = \begin{bmatrix} \mathbf{GC}_\beta \dfrac{\partial \mathbf{C}_\alpha}{\partial \rho_k} & \mathbf{0} \\ \mathbf{0} & \mathbf{0} \end{bmatrix} \tag{40}$$

2

3 Inserting equations (36)-(40) into equation (35), it can be seen that $\frac{\partial E}{\partial \rho_k}$ is the only

4 unknown quantity. Differentiating equation (10) with respect to the kth design variable,

5 yields

6

$$\frac{\partial E}{\partial \rho_k} = \left(\frac{\partial P_{\text{in}}^{\text{dir}}}{\partial \rho_k} n_{\text{m}} - \frac{\partial h_{\text{out}}^{\text{rev}}}{\partial \rho_k} E \right) / (h_{\text{out}}^{\text{rev}} + h_{\text{diss}}) \tag{41}$$

7 By using equations (11) and (13), the partial derivative terms on the right of equation (41)

8 can be written as

9

$$\frac{\partial P_{\text{in}}^{\text{dir}}}{\partial \rho_k} = \frac{\omega}{2} \sum_{ij} \text{Im}\{\mathbf{D}_{\text{dir},ij}\} \left(\frac{\partial \mathbf{S}_{uu}^{\text{ext}}}{\partial \rho_k} \right)_{ij} \tag{42}$$

10

$$\frac{\partial h_{\text{out}}^{\text{rev}}}{\partial \rho_k} = \frac{2}{\pi} \text{Re} \left\{ -\mathrm{i} \sum_{ij} \mathbf{C}_{\text{sa},ij} \left(\frac{\partial \mathbf{Y}_{up}}{\partial \rho_k} \right)_{ij}^* \right\} \tag{43}$$

11

12 where $\frac{\partial \mathbf{S}_{uu}^{\text{ext}}}{\partial \rho_k}$ can be obtained from equation (36).

13   The solution procedure for the sensitivity analysis of objective function is

14 summarized below:

15 (i) The plate energy sensitivity with respect to design variables $\frac{\partial E}{\partial \rho_k}$ is obtained by

16   inserting equations (42) and (43) into equation (41);

17 (ii) Substituting equation (41) into equation (37), and using equations (35) and (36), $\frac{\partial \mathbf{S}_{qq}}{\partial \rho_k}$

1   is then calculated;

2   (iii) Inserting equations (27)-(29) into equation (26), and using equations (33)-(35), one

3   can obtain the sensitivity of the cross-spectrum matrix of sound pressure at inner

4   points with respect to design variables $\frac{\partial \mathbf{S}_{pp}^{\text{in}}}{\partial \rho_k}$.

5   (iv) The objective function sensitivity with respect to design variables is calculated by

6   using equation (26).

7   The sensitivity of the constraint function in the optimization model equation (22)

8   with respect to the kth design variable ρ_k equals V_k^0.

9

10 **4 Numerical example**

11   A simple verification example consisting of two thin plates and an acoustic cavity,

12 as shown in Fig. 3, is presented for illustrating the validity of the proposed topology

13 optimization model. The acoustic cavity is comprised of air and has geometrical

14 dimensions 0.7 m by 1 m by 0.5 m. The sound speed and mass density of the air are

15 $c_0 = 340$ m/s and $\rho_a = 1.225$ kg/m^3, respectively. Two thin plates with the same

16 dimensions of 0.7 m by 1.0 m by 1 mm are connected respectively to the front and rear

17 surfaces of the acoustic cavity (the gray areas in Fig. 3). The edges of the two plates are

18 all simply supported, and the in-plane deformation of the two plates is ignored. The two

19 plates are made of aluminum, of which the mass density, Young's modulus, Poisson's

20 ratio and damping loss factor are 2700 kg/m^3, 7.1×10^{10} Pa, 0.33 and 0.01, respectively.
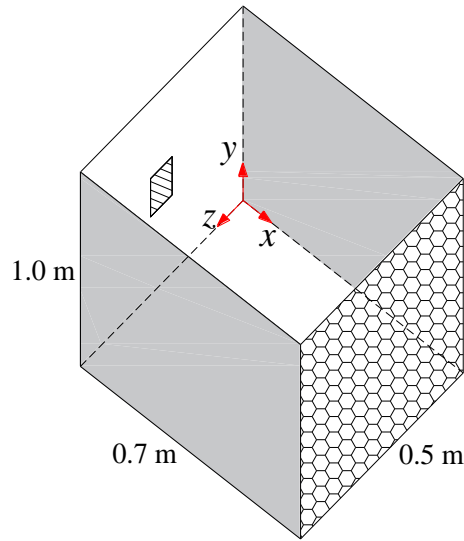
1

2   Fig. 3   Geometric diagram of the vibro-acoustic system. Diagonally hashed area, the

3   region subjected to velocity excitation; gray area, two plates coupled to the acoustic

4   cavity; hexagon filled area, the design domain of sound absorbing material layer; other

5   areas, acoustically rigid walls.

6

7   The design domain of a sound absorbing layer is connected to the right surface of

8   the acoustic cavity (the hexagon filled area in Fig. 3). A unit velocity excitation is applied

9   over a square region (see the diagonal area in Fig. 3) of 0.04 m^2 on the left surface of the

10   acoustic cavity located at the point (0, 0.5, 0.25). The other areas are considered to be

11   acoustically rigid.

12   **4.1 Response analysis for the mid-frequency vibration of the vibro-**

13   **acoustic system**

14   In order to show the efficiency of the hybrid BE-SEA method, the responses of the

15   vibro-acoustic system calculated by employing the hybrid BE-SEA method are compared

23

1   with those calculated by using Monte Carlo simulation.

2   The impedance of the sound absorbing material is set to be a large real number 10^{40},

3   and all element-relative densities of the sound absorbing material in the design domain

4   are set to be 1. The frequency range considered here is from 1 Hz to 400 Hz with a

5   frequency step of 1 Hz. Since the acoustic cavity and each thin plate respectively have 7

6   and 79 modes below 400 Hz, which illustrates the modal density of the acoustic cavity

7   and each plate are significantly different, the systems will exhibit typical mid-frequency

8   vibration behavior consisting of a deterministic acoustical behavior and a statistical

9   structural behavior, within the frequency range of interest. In the hybrid BE-SEA model,

10   the acoustic cavity is modeled by using the BE method, while the two plates are modeled

11   by using SEA. A pure FE model is employed in the Monte Carlo simulation, and a regular

12   fine FE mesh requires to be established to capture detailed deformation. Considering the

13   influence of the uncertainties of the system, an ensemble consisting of 500 samples is

14   generated by randomly choosing 200 points within each plate and adding 0.1% of the

15   mass of one plate at each point.

16   It is important to point out that appropriate element sizes should be chosen for the

17   parts modeled using element-based techniques in the two methods, i.e. at least six element

18   per wavelength. Table 1 gives the details of the parts modeled using element-based

19   techniques and the time cost by two methods. As can be seen from Table 1, the minimum

20   number of DOFs and time cost are required for the hybrid FE-SEA method. The hybrid

1 implementations and the Monte Carlo simulation are performed single-threaded in Julia

2 (v0.6.3.1) on a 3.3 GHz Intel Xeon-based system with a Windows operating system.

3   A comparison of the PSDSP at the point (0.3, 0.6, 0.4) inside the acoustic cavity

4 calculated by using the hybrid BE-SEA method and the Monte Carlo simulation is shown

5 in Fig. 4. As can be seen from Fig. 4, the resulting curves of 500 samples are concentrated

6 at lower frequencies, which confirms that the system uncertainties have little impact on

7 the system responses when the system is subjected to long wavelength deformation. In

8 consideration of the sufficient uncertainty the hybrid BE-SEA has assumed over the entire

9 frequency range, significant discrepancies can be observed between the results calculated

10 with the two methods at lower frequencies.

11   Table 1   Details of two analysis models

Analysis model		Element type	Element size (m)	Number of elements per wavelength at 400Hz	Number of DOFs	Calculation time (h)
Hybrid BE-SEA	Cavity	4-node quadrilateral	0.050	17	1242	7.9
	Direct field	4-node quadrilateral	0.025	6	1189×2	
Monte Carlo simulation	Cavity	8-node hexahedral	0.025	34	24969	61.4
	Plate	4-node quadrilateral	0.020	6	5508×2	
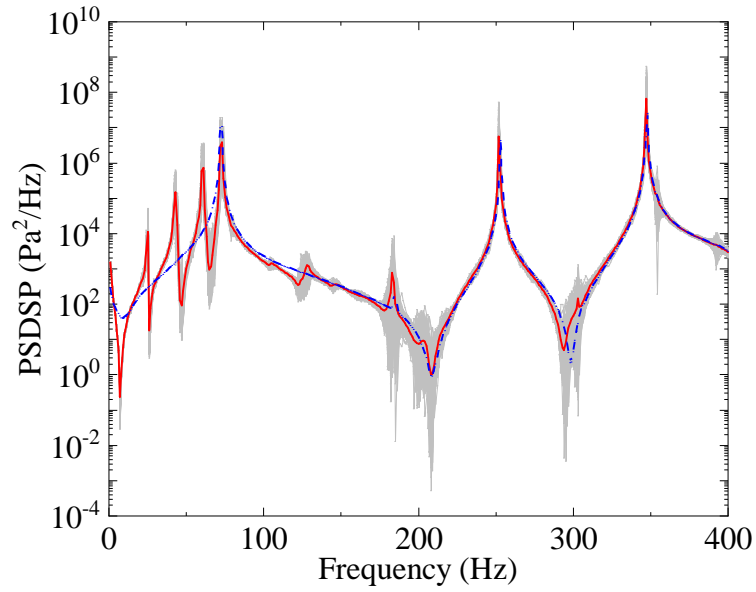
Fig. 4   PSDSP at a point inside the acoustic cavity with coordinates (0.3, 0.6, 0.4). Fine

solid gray lines, computed using Monte Carlo approach for 500 realizations of

ensemble; bold solid red line, ensemble average of Monte Carlo results; bold dash blue

line, ensemble average computed using Hybrid BE-SEA method.

As the frequency increases, the system response becomes very sensitive to the

uncertainties of the system, and the resulting curves of 500 samples become dispersed.

The hybrid BE-SEA method predicts well the average trend of the pure FE method

calculations with perturbed plate mass at higher frequencies. Furthermore, according to

the principles of the hybrid BE-SEA method, there is sufficient uncertainty in a statistical

subsystem. Hence, it should be pointed out that the average of the Monte Carlo results,

which cannot involve all uncertainties (sufficient uncertainty), may have discrepancies

with the results obtained by hybrid BE-SEA method even at some higher frequencies

1 (Cotoni et al. 2007; Shorter and Langley 2005b).

2 In this paper, the discrepancies at lower frequencies may be neglected since the

3 attention is only on the mid-frequency vibration of vibro-acoustic systems.

4

5 **4.2 Sensitivity analysis and topology optimization of sound absorbing**

6 **layer for mid-frequency vibration of the vibro-acoustic system**

7 Setting the excitation frequency to be 415 Hz, the partition of the system can be

8 performed by wavelength analysis for the acoustic cavity and the two plates. Here, the

9 acoustic cavity is modeled using the BE method, while the two plates are modeled using

10 SEA. Element sizes chosen for the parts modeled using element-based techniques are the

11 same as those in Table.1. The design domain is discretized by 200 (20×10) uniform-

12 sized square elements. Hence there are 200 design variables $\rho_k (k = 1, 2, \ldots, 200)$. The

13 method of moving asymptotes (MMA) (Svanberg 1987, 2002; Johnson 2008, 2014) is

14 employed to update the design variables. The optimization process is stopped when the

15 relative difference of the PSDSP between two adjacent iteration steps is less than 10^{-6}.

16 Sensitivity analysis for the PSDSP is considered first. The point (0.35, 0.50, 0.25) is

17 adopted as the reference point. The impedance of the sound absorbing material is set to

18 be $Z_0 = 975 + 8798i$ kg / (m^{2}s) (see Siemens Product Lifecycle Management Software

19 Inc 2014), and all element-relative densities of the sound absorbing material in the design

20 domain are set to be 0.6. The relative errors of the sensitivities of the objective function

1 with respect to the design variables $\partial \tilde{S}^{in}_{pp}/\partial \rho_k (k = 1, 2, \ldots, 200)$, calculated by using the

2 present method and the finite difference method (FDM) with 10^{-4} perturbation, are given

3 in Fig. 5.

4   As can be seen from Fig. 5, the comparison shows good agreement. The FDM

5 requires one solution of the linear system of equations for the original value plus one

6 solution (or two if using a central perturbation method) for each design variable. For the

7 present method, one solution of the linear system of equations for the original value is

8 required, and then, according to section 3.2, the derivative (sensitivity) can be calculated

9 directly by a few matrix product operations, without other solutions of the linear system

10 of equations for each design variable. Therefore, compared with FDM, the present method

11 requires less computation time.

12
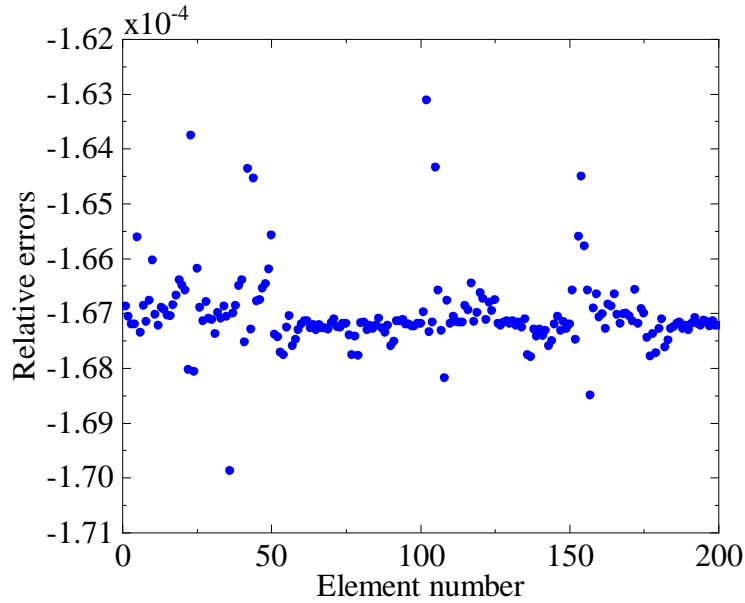
13   Fig.5   Relative errors of the sensitivities of the PSDSP at the reference point with

14   respect to the element relative density of sound absorbing material.

1   In the following, topology optimization for the vibro-acoustic system is considered.

2   The point (0.60, 0.50, 0.25) is adopted as the reference point. The impedance of the sound

3   absorbing material is set as $Z_0 = 4\rho_a c_0$. All initial design variables are set to be 0.4, and

4   the upper limit of the volume fraction of the sound absorbing material is given as $f_V = 0.5$.

5   The optimization procedure converged after 21 iterations, and the iteration histories of

6   the objective function and volume fraction are shown in Fig. 6. As can be seen, the PSDSP

7   decreases significantly from 196065.61 Pa^2/Hz in the initial design to 52063.696 Pa^2/Hz

8   in the final optimized design, and the volume fraction of the sound absorbing material

9   reaches the upper limit. The sound absorbing layer layout and the contour of the PSDSP

10   of the design domain for the initial and the optimized design are shown in Fig. 7. As can

11   be seen, the sound absorbing material is concentrated in the places where there is a high

12   PSDSP in the initial design, which indicates that incident sound waves reflect strongly at
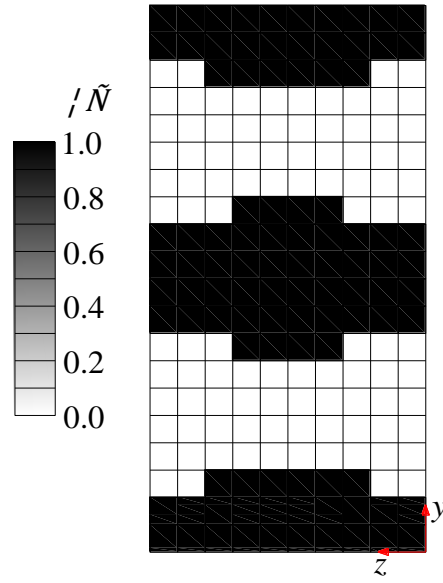

13
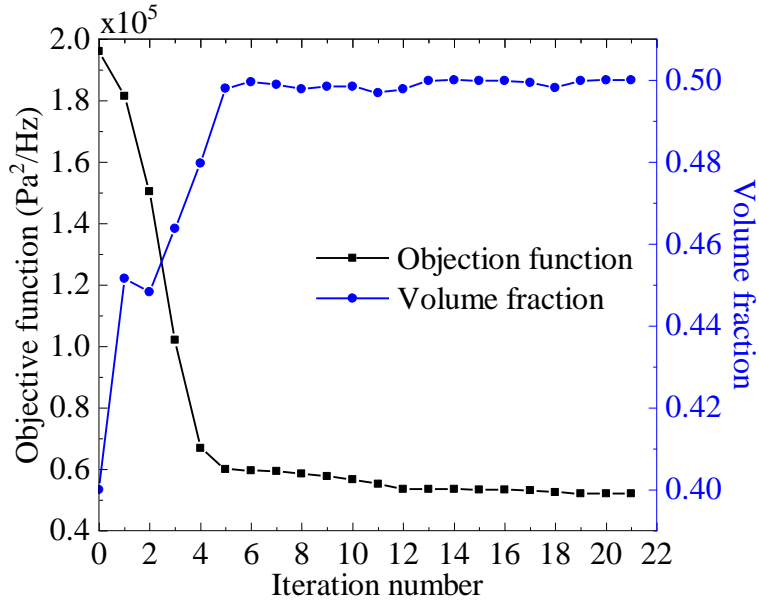
14   Fig. 6   Iteration histories of objective function and volume fraction.

1
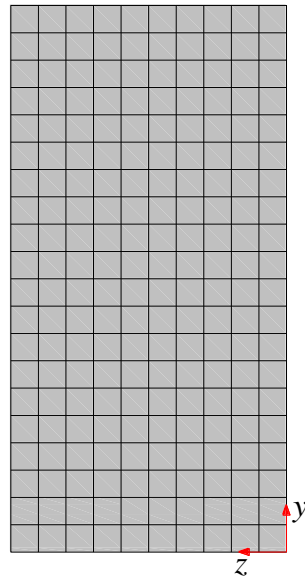
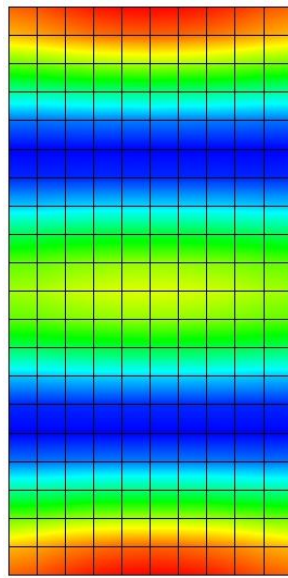2   (a) Initial design   (b) Optimized design
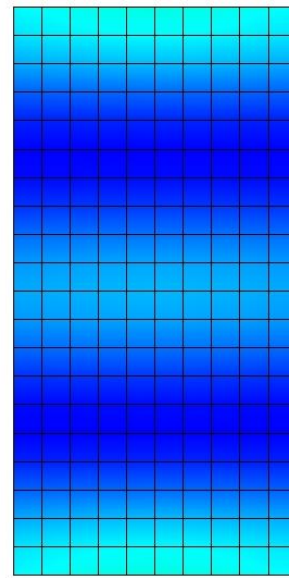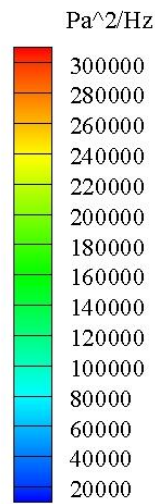
3

4   (c) Initial design   (d) Optimized design

5   Fig. 7   Distributions of sound absorbing material for (a) the initial design, (b) the

6   optimized design. The colorbar shows relative density of the sound absorbing material.

7   Contours of the PSDSP for (c) the initial design, (d) the optimized design. The colorbar

8   shows the PSDSP of the design domain.

1   these areas. It can be seen from Fig. 7c and d that the PSDSP of the overall design domain

2   has significantly reduced.

3   Fig. 8 shows curves of PSDSP at the reference point in the frequency range of 300

4   Hz - 500 Hz for the initial and optimized designs. As can be seen, the natural frequencies

5   of the system remain unchanged in the optimization process. Although the excitation

6   frequency selected in the optimization process is 415 Hz, the PSDSP at the reference point

7   decreases over the whole frequency range. However, it is important to point out that the

8   dynamic optimization problem for a vibro-acoustic system is highly nonconvex. A locally

9   optimized design is generally obtained by using a gradient-based mathematical

10   programming algorithm, but such solutions may provide helpful guidance at the

11   conceptual design stage.
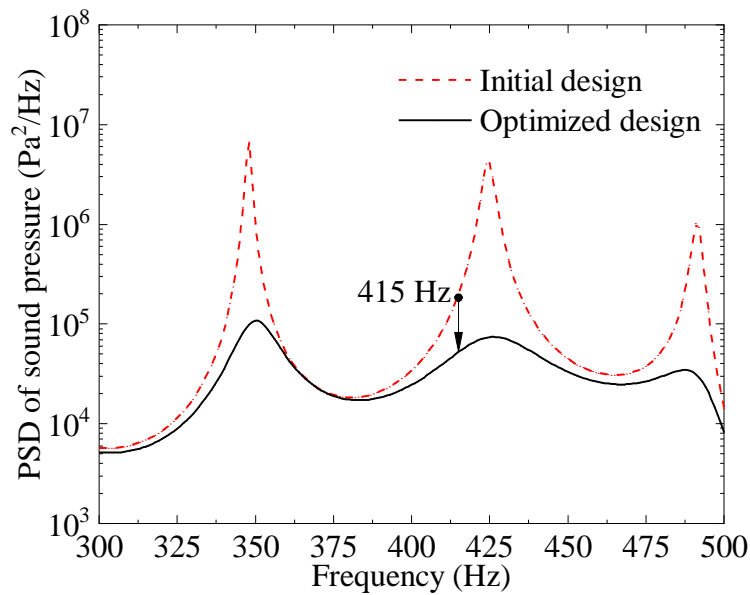

12

13   Fig. 8   Curves of PSDSP at the reference point in the frequency range of 300 Hz - 500

14   Hz for the initial and optimized designs.

1   **4.3 Influence of excitation frequencies on optimized designs**

2   In the following, the influence of excitation frequencies on optimized designs is

3   considered. The point (0.60, 0.50, 0.25) is adopted as the reference point. The impedance

4   of the sound absorbing material is set as $Z_0 = 4\rho_a c_0$. All initial design variables are set

5   to be 0.4, and the upper limit of the volume fraction of the sound absorbing material is

6   given as $f_V = 0.5$. The optimization process is performed by selecting the excitation

7   frequencies as 348 Hz, 381 Hz, 425 Hz, 466 Hz, 491 Hz, 300 Hz, 400 Hz and 500 Hz. It

8   can be seen from Fig. 8 that the first five selected frequencies correspond to the three

9   peaks and two valleys of the curve of the PSDSP, and the last three selected frequencies

10   correspond to the beginning, middle and end points of the frequency range of interest.

11

12

13   (a) 348 Hz   (b) 381 Hz   (c) 425 Hz
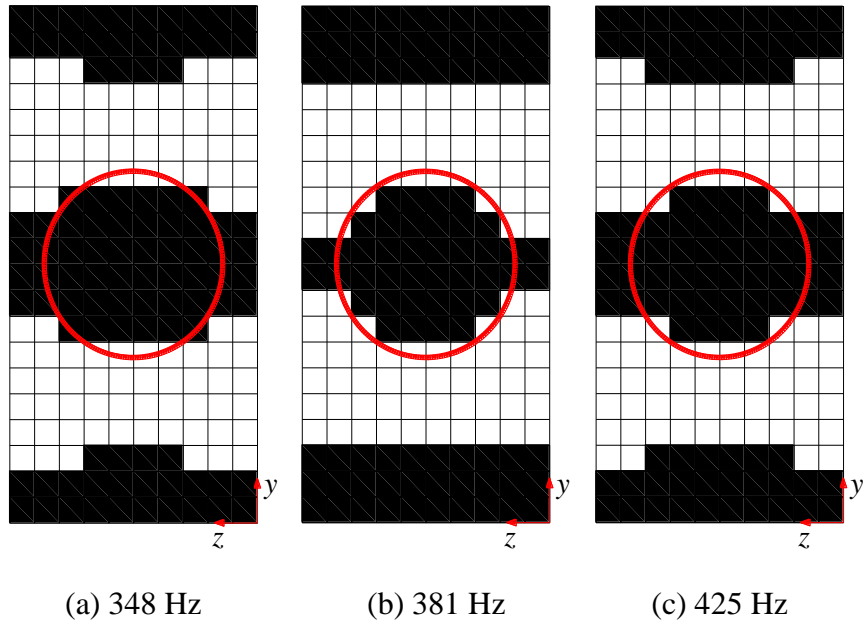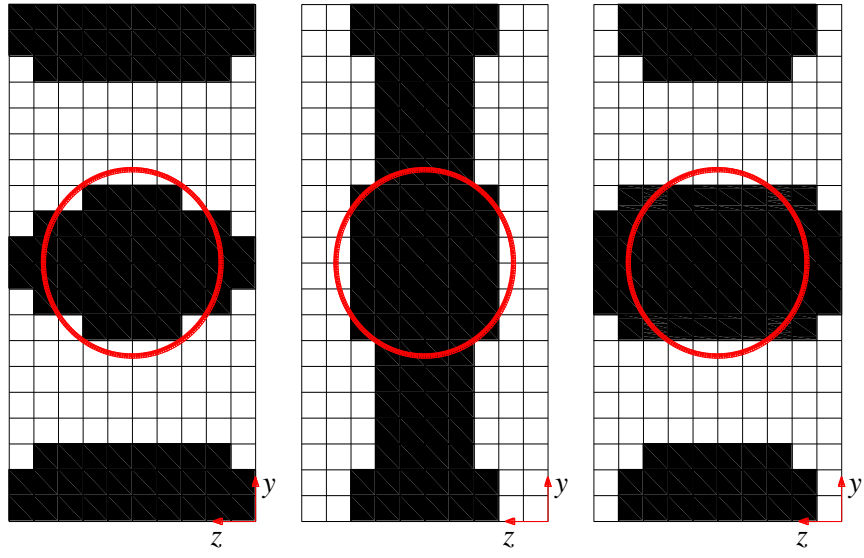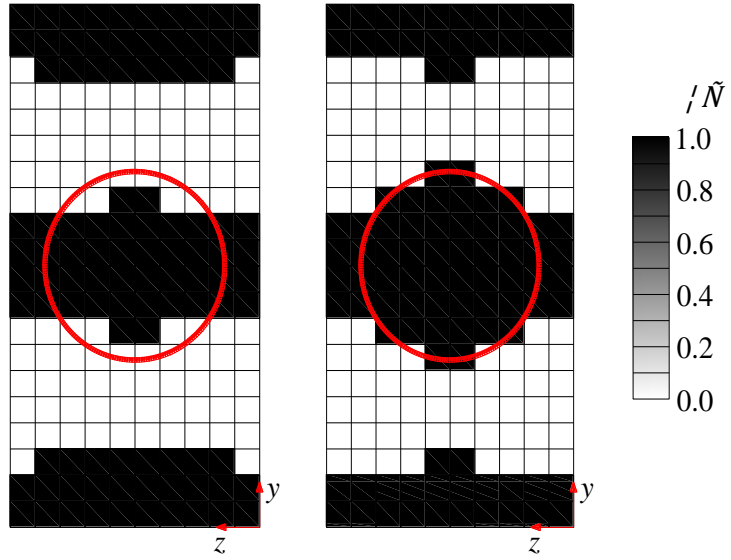
(d) 466 Hz   (e) 491 Hz   (f) 300 Hz

(g) 400 Hz   (h) 500 Hz

Fig. 9   Optimized design under eight selected excitation frequencies. The colorbar

shows relative density of the sound absorbing material.

The optimized designs obtained under each excitation frequency are shown in Fig.

9. As can be seen, the topology optimization process gives essentially the same optimized

designs under most selected excitation frequencies, except for 491 Hz. Moreover,

although the optimized design obtained under excitation frequency 491 Hz is obviously

different from that obtained under the other seven selected excitation frequencies, the

central area of the design domain (the area drawn by the red circle in Fig. 9) is always

covered with sound absorbing material, which indicates that incident sound waves reflect

strongly at the central area. This is natural since the direction of the velocity excitation

points exactly to the central area of the design domain.

The first five optimized designs are further studied because the last three optimized

designs are very similar to the first three optimized designs. The curves of PSDSP at the

reference point in the frequency range of 300 Hz - 500 Hz for the initial and first five

optimized designs are shown in Fig. 10. As can be seen, the PSDSP at the reference point

decreases over the whole frequency range for the first five optimized designs. In addition,

the five curves of PSDSP corresponding to the first five optimized designs are very close,

which illustrates the importance of the central area of the design domain.

Consider now the topology optimization over the whole frequency band. Selecting

3 sampling frequencies (348 Hz, 425 Hz and 491 Hz) in the frequency band of interest,

an envelope of the objection function, which is constructed by using a composite

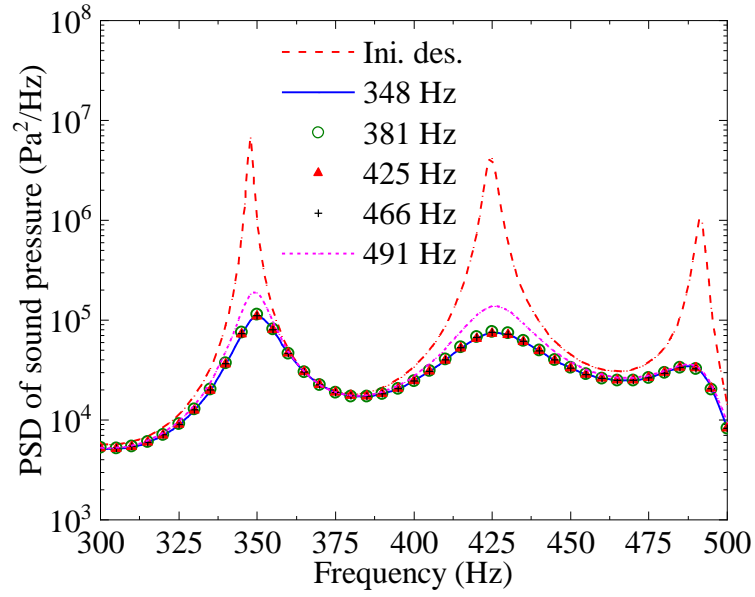Kreisselmeier - Steinhauser objective function (Kreisselmeier and Steinhauser 1979;

34

1

2

3   Fig. 10   Curves of PSDSP at the reference point in the frequency range of 300 Hz - 500

4   Hz for the initial and first five optimized designs.
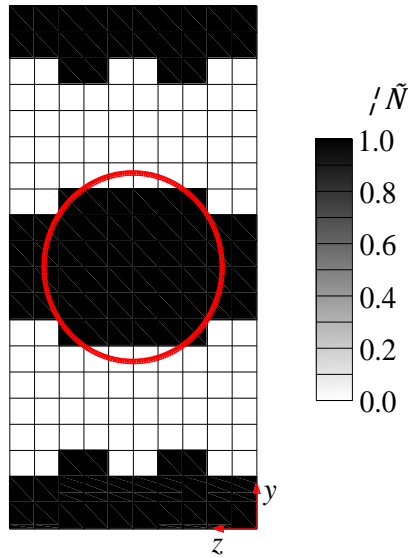
5

6

7   Fig. 11   Optimized design obtained using an envelope function as the objective

8   function. The colorbar shows relative density of the sound absorbing material.

9

1   Wrenn 1989) with the aggregation parameter η =1000, is taken as the objective function

2   to be minimized.

3   The optimized design obtained using an envelope function over the whole frequency

4   range as the objective function is shown in Fig. 11. As can be seen, it is almost the same

5   as the optimized design obtained in Fig. 8 under 348 Hz or 425 Hz. Fig. 12 gives the

6   comparisons between the PSDSP at the reference point in the frequency range of 300 -

7   500 Hz for the initial and the optimized designs. As can be seen from Fig. 12, the PSDSP

8   at the reference point decreases over the whole frequency range for the optimized design

9   obtained using an envelope function as the objective function. And the optimized design

10   obtained using an envelope function, not surprisingly, gives almost the same PSDSP at

11   the reference point as the optimized design obtained under 348 Hz or 425 Hz.

12
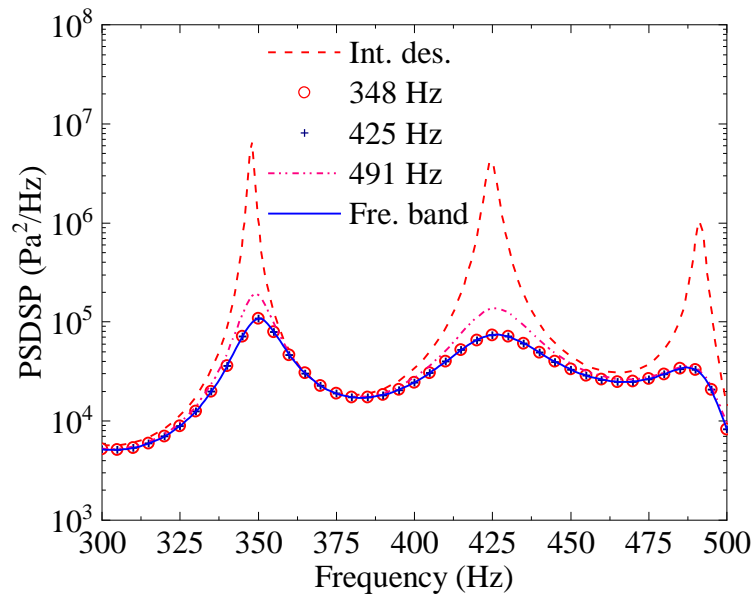
13   Fig. 12   Curves of PSDSP at the reference point in the frequency range of 300 - 500 Hz

14   for the initial and optimized designs.

5 Conclusions

This paper performs the sensitivity analysis and topology optimization of a sound absorbing layer for minimizing the PSDSP at a specified point in the acoustic cavity when a vibro-acoustic system exhibits mid-frequency behavior. In the topology optimization model, an artificial sound absorbing material model is employed using the SIMP approach and the relative densities of the sound absorbing material are taken as design variables. The PSDSP of the acoustic cavity are calculated by using a hybrid BE-SEA method. In this context, the sensitivity analysis scheme of the PSDSP at a given reference point is developed by using the direct differentiation method. The optimized designs obtained under different excitation frequencies and using an envelope function as the objective function are also compared. The optimization process gives essentially the same optimized designs over a relatively wide frequency range. Moreover, due to the strong reflection of sound waves, the central area in the design domain which faces the region at which the velocity is applied is always covered with sound absorbing material.

References

Akl W, El-Sabbagh A, Al-Mitani K, Baz A (2009) Topology optimization of a plate coupled with acoustic cavity. International Journal of Solids and Structures 46:2060-2074

Allaire G, Jouve F, Toader AM (2004) Structural optimization using sensitivity analysis and a level-set method. Journal of Computational Physics 194(1): 363-393

Bathe KJ (2008) Finite Element Method. John Wiley & Sons, Inc., Hoboken

Bendsøe MP (1989) Optimal shape design as a material distribution problem. Structural Optimization 1(4): 193-202

Bendsøe MP, Kikuchi N (1988) Generating optimal topologies in structural design using a homogenization method. Computer Methods in Applied Mechanics and Engineering 71(2): 197-224

Bendsøe MP, Sigmund O (2003) Topology Optimization, Theory, Methods and Applications. Springer, Berlin

Christensen ST, Sorokin SV, Olhoff N (1998a) On analysis and optimization in structural acoustics - Part I: Problem formulation and solution techniques. Structural Optimization 16(2-3): 83-95

Christensen ST, Sorokin SV, Olhoff N (1998b) On analysis and optimization in structural acoustics - Part II: Exemplifications for axisymmetric structures. Structural Optimization 16(2-3): 96-107

1   Christiansen RE, Lazarov BS, Jensen JS, Sigmund O (2015) Creating geometrically

2   robust designs for highly sensitive problems using topology optimization. Structural

3   and Multidisciplinary Optimization 52: 737-754

4   Christiansen RE, Sigmund O (2015) Experimental validation of a topology optimized

5   acoustic cavity. Journal of the Acoustical Society of America 138: 3470-3474

6   Ciskowski R, Brebbia C (1991) Boundary Element Methods in Acoustics. Computational

7   Mechanics Publications, Southampton

8   Cotoni V, Shorter P, Langley R (2007) Numerical and experimental validation of a hybrid

9   finite element - statistical energy analysis method. Journal of the Acoustical Society

10   of America 122(1): 259-270

11   Du J, Olhoff N (2007) Minimization of sound radiation from vibrating bi-material

12   structures using topology optimization. Structural and Multidisciplinary

13   Optimization 33(4-5): 305-321

14   Du J, Olhoff N (2010) Topological design of vibrating structures with respect to optimum

15   sound pressure characteristics in a surrounding acoustic medium. Structural and

16   Multidisciplinary Optimization 42(1): 43-54

17   Dühring MB, Jensen JS, Sigmund O (2008) Acoustic design by topology optimization.

18   Journal of Sound and Vibration 317(3-5): 557-575

19   Gao R, Zhang Y, Kennedy D (2018) A hybrid boundary element-statistical energy

20   analysis for the mid-frequency vibration of vibro-acoustic systems. Computers and

Structures 203: 34-42

Goo S, Wang S, Kook J, Koo K, Hyun J (2017) Topology optimization of bounded acoustic problems using the hybrid finite element-wave based method. Computer Methods in Applied Mechanics and Engineering 313: 834-856

Harari I, Avraham D (1997) High-order finite element methods for acoustic problems. Journal of Computational Acoustics 5(1): 33-51

Herrin DW, Martinus F, Wu TW, Seybert AF (2003) A new look at the high frequency boundary element and Rayleigh integral approximations. Society of Automotive Engineers, Technical Paper 2003-01-1451

Hinke L, Dohnal F, Mace BR, Waters TP, Ferguson NS (2009) Component mode synthesis as a framework for uncertainty analysis. Journal of Sound and Vibration 324(1-2): 161-178

Ji L, Mace BR, Pinnington RJ (2006) A mode-based approach for the mid-frequency vibration analysis of coupled long- and short-wavelength structures. Journal of Sound and Vibration 289(1-2): 148-170

Johnson SG (2008) The Nlopt nonlinear-optimization package. https://nlopt.readthedocs. io/en/latest/

Johnson SG (2014) Package to call the NLopt nonlinear-optimization library from the Julia language. https://github.com/JuliaOpt/NLopt.jl

Keane AJ, Price WG (1987) Statistical energy analysis of strongly coupled systems.

1   Journal of Sound and Vibration 117(2): 363-386

2   Kook J, Koo K, Hyun J, Jensen JS, Wang S (2012) Acoustical topology optimization for

3   Zwicker's loudness model - Application to noise barriers. Computer Methods in

4   Applied Mechanics and Engineering 237-240: 130-151

5   Kreisselmeier G, Steinhauser R (1979) Systematic control design by optimizing a vector

6   performance index. In: IFAC symposium on computer-aided design of control

7   systems, international federation of active controls. Zurich, Switzerland

8   Ladeveze P, Barbarulo A, Riou H, Kovalevsky L (2012) Mid-Frequency - CAE

9   Methodologies for Mid-Frequency Analysis in Vibration and Acoustics. Leuven

10   University Press, Leuven

11   Langley RS (1989a) A general derivation of the statistical energy analysis equations for

12   coupled dynamic systems. Journal of Sound and Vibration 135(3): 499-508

13   Langley RS (1989b) Application of the dynamic stiffness method to the free and forced

14   vibrations of aircraft panels. Journal of Sound and Vibration 135(2): 319-331

15   Langley RS (1992) A wave intensity technique for the analysis of high frequency

16   vibrations. Journal of Sound and Vibration 159(3): 483-502

17   Lax M, Feshbach H (1947) On the radiation problem at high frequencies. Journal of the

18   Acoustical Society of America 19(4): 682-690

19   Lyon RH, DeJong RG (1995) Theory and Application of Statistical Energy Analysis. 2nd

20   ed., Butterworth-Heinemann, Boston

1   Ma Y, Zhang Y, Kennedy D (2015a) A hybrid wave propagation and statistical energy

2   analysis on the mid-frequency vibration of built-up plate systems. Journal of Sound

3   and Vibration 352: 63-79

4   Ma Y, Zhang Y, Kennedy D (2015b) A symplectic analytical wave based method for the

5   wave propagation and steady state forced vibration of rectangular thin plates. Journal

6   of Sound and Vibration 339: 196-214

7   Mace BR (2005) Statistical energy analysis: coupling loss factors, indirect coupling and

8   system modes. Journal of Sound and Vibration 279(1-2): 141-170

9   Maxit L, Guyader JL (2003) Extension of SEA model to subsystems with non-uniform

10   modal energy distribution. Journal of Sound and Vibration 265(2): 337-358

11   Muthalif AGA, Langley RS (2012) Active control of high-frequency vibration:

12   Optimisation using the hybrid modelling method. Journal of Sound and Vibration

13   331(13): 2969-2983

14   Pluymers B, Van Hal B, Vandepitte D, Desmet W (2007) Trefftz-based methods for time-

15   harmonic acoustics. Archives of Computational Methods in Engineering 14(4): 343-

16   381

17   Shorter PJ, Langley RS (2005a) On the reciprocity relationship between direct field

18   radiation and diffuse reverberant loading. Journal of the Acoustical Society of

19   America 117(1): 85-95

20   Shorter PJ, Langley RS (2005b) Vibro-acoustic analysis of complex systems. Journal of

Sound and Vibration 288(3): 669-699

Shu L, Wang MY, Ma Z (2014) Level set based topology optimization of vibrating structures for coupled acoustic-structural dynamics. Computers and Structures 132: 34-42

Siemens Product Lifecycle Management Software Inc (2014) LMS Virtual. Lab On-line help. Munich: Siemens AG

Sigmund O (2001) A 99 line topology optimization code written in Matlab. Structural and Multidisciplinary Optimization 21(2): 120-127

Simmons C (1991) Structure-borne sound transmission through plate junctions and estimates of SEA coupling loss factors using the finite element method. Journal of Sound and Vibration 144(2): 215-227

Steel JA, Craik RJM (1994) Statistical energy analysis of structure-borne sound transmission by finite element methods. Journal of Sound and Vibration 178(4): 553-561

Svanberg K (1987) The method of moving asymptotes - a new method for structural optimization. International Journal for Numerical Methods in Engineering 24(2): 359-373

Svanberg K (2002) A class of globally convergent optimization methods based on conservative convex separable approximations. SIAM Journal on Optimization 12(2): 555-573

Van Vinckenroy G, De Wilde WP (1995) The use of Monte Carlo techniques in statistical finite element methods for the determination of the structural behaviour of composite materials structural components. Composite Structures 32(1-4): 247-253

Vergote K, Van Genechten B, Vandepitte D, Desmet W (2011) On the analysis of vibro-acoustic systems in the mid-frequency range using a hybrid deterministic - statistical approach. Computers and Structures 89(11-12): 868-877

Wang MY, Wang X, Guo D (2003) A level set method for structural topology optimization. Computer Methods in Applied Mechanics and Engineering 192(1-2): 227-246

Wrenn G (1989) An indirect method for numerical optimization using the Kreisselmeier - Steinhauser function. Contractor report NASA CR - 4220, NASA Langley Research Center, Hampton, VA, USA

Wu TW (2000) Boundary Element Acoustics: Fundamentals and Computer Codes. WIT, Southampton

Yoon GH, Jensen JS, Sigmund O (2007) Topology optimization of acoustic-structure interaction problems using a mixed finite element formulation. International Journal for Numerical Methods in Engineering 70(9): 1049-1075

Zhang X, Kang Z (2013) Topology optimization of damping layers for minimizing sound radiation of shell structures. Journal of Sound and Vibration 332(10): 2500-2519

Zhao W, Chen L, Zheng C, Liu C, Chen H (2017) Design of absorbing material distribution for sound barrier using topology optimization. Structural and

1   Multidisciplinary Optimization 56: 315-329

2   Zhao X, Vlahopoulos N (2000) Hybrid finite element formulation for mid-frequency

3   analysis of systems with excitation applied on short members. Journal of Sound and

4   Vibration 237(2): 181-202

5   Zhou M, Rozvany GIN (1991) The COC algorithm, Part II: Topological, geometry and

6   generalized shape optimization. Computer Methods in Applied Mechanics and

7   Engineering 89(1-3): 309-336

8   Zhu D, Chen H, Kong X, Zhang W (2014) A hybrid finite element-energy finite element

9   method for mid-frequency vibrations of built-up structures under multi-distributed

10   loadings. Journal of Sound and Vibration 333(22): 5723-5745

11   Zienkiewicz OC, Taylor RL (2000) The Finite Element Method. 5th ed., Butterworth-

12   Heinemann, Oxford

13